Supplement of Clim. Past, 21, 1043–1060, 2025
https://doi.org/10.5194/cp-21-1043-2025-supplement

Climate of the Past
Open Access

Supplement of

Closing the Plio-Pleistocene ^{13}C cycle in the 405 kyr periodicity by isotopic signatures of geological sources

Peter Köhler

Correspondence to: Peter Köhler (peter.koehler@awi.de)

References

Barth, A. M., Clark, P. U., Bill, N. S., He, F., and Pisias, N. G.: Climate evolution across the Mid-Brunhes Transition, Climate of the Past, 14, 2071–2087, https://doi.org/10.5194/cp-14-2071-2018, 2018.

Bereiter, B., Eggleston, S., Schmitt, J., Nehrbass-Ahles, C., Stocker, T. F., Fischer, H., Kipfstuhl, S., and Chappellaz, J.: Revision of the EPICA Dome C CO_2 record from 800 to 600 kyr before present, Geophysical Research Letters, 42, 542–549, https://doi.org/10.1002/2014GL061957, 2015.

Bintanja, R. and van de Wal, R. S. W.: North American ice-sheet dynamics and the onset of the 100,000-year glacial cycles, Nature, 454, 869–872, https://doi.org/10.1038/nature07158, 2008.

de Boer, B., Lourens, L. J., and van de Wal, R. S.: Persistent 400,000-year variability of Antarctic ice volume and the carbon cycle is revealed throughout the Plio-Pleistocene, Nature Communications, 5, 2999, https://doi.org/10.1038/ncomms3999, 2014.

Eggleston, S., Schmitt, J., Bereiter, B., Schneider, R., and Fischer, H.: Evolution of the stable carbon isotope composition of atmospheric CO_2 over the last glacial cycle, Paleoceanography, 31, 434–452, https://doi.org/10.1002/2015PA002874, 2016.

EPICA-community-members: Eight glacial cycles from an Antarctic ice core, Nature, 429, 623–628, https://doi.org/10.1038/nature02599, 2004.

Flower, B. P., Oppo, D. W., McManus, J. F., Venz, K. A., Hodell, D. A., and Cullen, J. L.: North Atlantic intermediate to deep water circulation and chemical stratification during the past 1 Myr, Paleoceanography, 15, 388–403, https://doi.org/10.1029/1999PA000430, 2000.

Jouzel, J., Masson-Delmotte, V., Cattani, O., Dreyfus, G., Falourd, S., Hoffmann, G., Minster, B., Nouet, J., Barnola, J. M., Chappellaz, J., Fischer, H., Gallet, J. C., Johnsen, S., Leuenberger, M., Loulergue, L., Luethi, D., Oerter, H., Parrenin, F., Raisbeck, G., Raynaud, D., Schilt, A., Schwander, J., Selmo, E., Souchez, R., Spahni, R., Stauffer, B., Steffensen, J. P., Stenni, B., Stocker, T. F., Tison, J. L., Werner, M., and Wolff, E. W.: Orbital and millennial Antarctic climate variability over the last 800 000 years, Science, 317, 793–796, https://doi.org/10.1126/science.1141038, 2007.

Köhler, P.: Atmospheric CO_2 concentration based on boron isotopes versus simulations of the global carbon cycle during the Plio-Pleistocene, Paleoceanography and Paleoclimatology, 38, e2022PA004 439, https://doi.org/10.1029/2022PA004439, 2023.

Köhler, P. and Mulitza, S.: No detectable influence of the carbonate ion effect on changes in stable carbon isotope ratios (δ^{13}C) of shallow dwelling planktic foraminifera over the past 160 kyr, Climate of the Past, 20, 991–1015, https://doi.org/10.5194/cp-20-991-2024, 2024.

Köhler, P. and Munhoven, G.: Late Pleistocene carbon cycle revisited by considering solid Earth processes, Paleoceanography and Paleoclimatology, 35, e2020PA004 020, https://doi.org/10.1029/2020PA004020, 2020.

Köhler, P., de Boer, B., von der Heydt, A. S., Stap, L. S., and van de Wal, R. S. W.: On the state dependency of equilibrium climate sensitivity during the last 5 million years, Climate of the Past, 11, 1801–1823, https://doi.org/10.5194/cp-11-1801-2015, 2015.

Krauss, F., Baggenstos, D., Schmitt, J., Tuzon, B., A., M. J., Mächler, L., Silva, L., Grimmer, M., Capron, E., Stocker, T. F., Bauska, T. K., and Fischer, F.: Multiple sources of atmospheric CO_2 activated by AMOC recovery at the onset of interglacial MIS 9, Proceedings of the National Academy of Sciences, 122, e2423057 122, https://doi.org/10.1073/pnas.2423057122, 2025.

Lambert, F., Delmonte, B., Petit, J. R., Bigler, M., Kaufmann, P. R., Hutterli, M. A., Stocker, T. F., Ruth, U., Steffensen, J. P., and Maggi, V.: Dust-climate couplings over the past 800,000 years from the EPICA Dome C ice core, Nature, 452, 616–619, https://doi.org/10.1038/nature06763, 2008.

Laskar, J., Robutel, P., Joutel, F., Gastineau, M., Correia, A. C. M., and Levrard, B.: A long term numerical solution for the insolation quantities of the Earth, Astronomy and Astrophysics, 428, 261–285, https://doi.org/10.1051/0004-6361:20041335, 2004.

Lisiecki, L. E.: Atlantic overturning responses to obliquity and precession over the last 3 Myr, Paleoceanography, 29, 71–86, https://doi.org/10.1002/2013PA002505, 2014.

Lisiecki, L. E. and Raymo, M. E.: A Pliocene-Pleistocene stack of 57 globally distributed benthic δ^{18}O records, Paleoceanography, 20, PA1003, https://doi.org/10.1029/2004PA001071, 2005.

Martinez-Garcia, A., Rosell-Mele, A., Jaccard, S. L., Geibert, W., Sigman, D. M., and Haug, G. H.: Southern Ocean dust-climate coupling over the past four million years, Nature, 476, 312–315, https://doi.org/10.1038/nature10310, 2011.

McManus, J. F., Oppo, D. W., and Cullen, J. L.: A 0.5-million-year record of millennial-scale climate variability in the North Atlantic, Science, 283, 971–975, https://doi.org/10.1126/science.283.5404.971, 1999.

Poore, H. R., Samworth, R., White, N. J., Jones, S. M., and McCave, I. N.: Neogene overflow of Northern Component Water at the Greenland-Scotland Ridge, Geochem. Geophys. Geosyst., 7, Q06 010, https://doi.org/10.1029/2005GC001085, 2006.

Wright, A. K. and Flower, B. P.: Surface and deep ocean circulation in the subpolar North Atlantic during the mid-Pleistocene revolution, Paleoceanography, 17, 1068, https://doi.org/10.1029/2002PA000782, 2002.

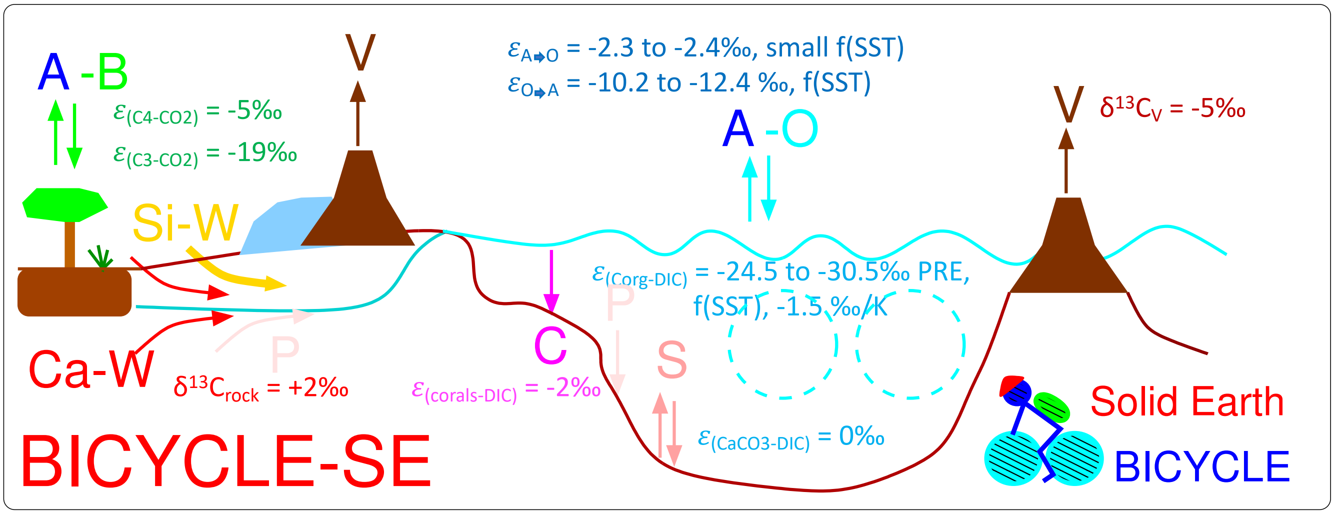

Figure S1. Sketch of the Box model of the isotopic carbon cycle, version solid Earth (BICYCLE-SE), taken from Köhler and Mulitza (2024). V: outgassing of CO_2 from volcanoes on land potentially and temporally overlain by land ice and from hot spot island volcanoes (and mid ocean ridges, not shown) influenced by changing sea level; C: shallow water carbonate deposition due to coral reef growth; Si-W: silicate weathering and Ca-W: carbonate weathering with different sources of C, but both delivering HCO_3^--ions into the ocean; P: PO_4^{3-} riverine input and sedimentary burial; S: $CaCO_3$ sedimentation and dissolution. A-B: atmosphere-biosphere exchange of CO_2; A-O: atmosphere-ocean exchange of CO_2. The cyan-coloured broken circles mimic the two overturning cell in the Atlantic and Indo-Pacific Ocean. The isotopic fractionation ε during exchange processes, or the prescribed δ^{13}C of external fluxes are given, summarising the parametrisation of the ^{13}C cycle within the model.

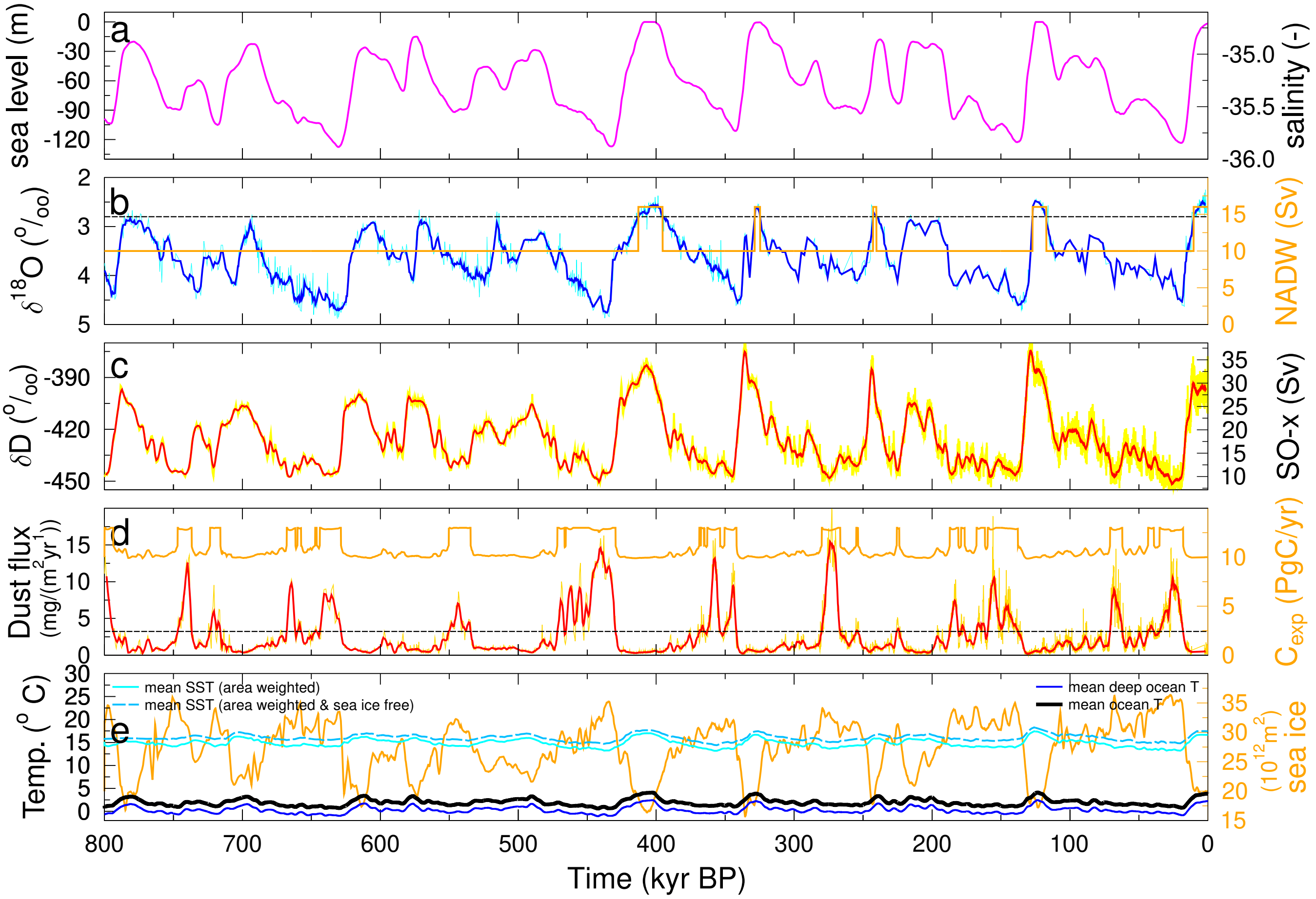

Figure S2. Time-dependent forcing of the model in scenario SEi (modified from Köhler and Munhoven (2020)). (a) Sea level following Bintanja and van de Wal (2008) resulting of corresponding mean ocean salinity (right y-axis). (b) North Atlantic Deep Water (NADW) formation is either in interglacial or glacial mode, following δ^{18}O in OPD980 (55°29′ N, 14°42′ W) (McManus et al., 1999; Flower et al., 2000; Wright and Flower, 2002), dotted line marks the threshold for switching between both states. (c) EDC ice core δD (EPICA-community-members, 2004; Jouzel et al., 2007) corrected for $\delta^{18}O_{sw}$, from which Southern Ocean sea surface temperatures (SST) and vertical mixing (SO-x: SO surface-to-deep ocean flux, right y-axis) is calculated. (d) Marine biology in the Southern Ocean (SO) is either Fe-limited or Fe-unlimited following dust fluxes in the EDC ice core (Lambert et al., 2008). The dotted line marks the threshold for switching between both states, leading to global integrated export production of organic matter at 100 m water depth (right y-axis). (e) Different ocean temperatures averaged within the model. Equatorial SST is taken from Barth et al. (2018). SST is calculated from all ocean surface boxes, deep ocean temperature from the boxes with water depths below 1000 m. The sea ice free SST is relevant for air-sea gas exchange. Right y-axis: global integrated sea ice area. In subfigures b–d original data (thin lines) and 3-kyr-running mean (bold lines) are shown. BICYCLE-SE is forced by the running-mean data.

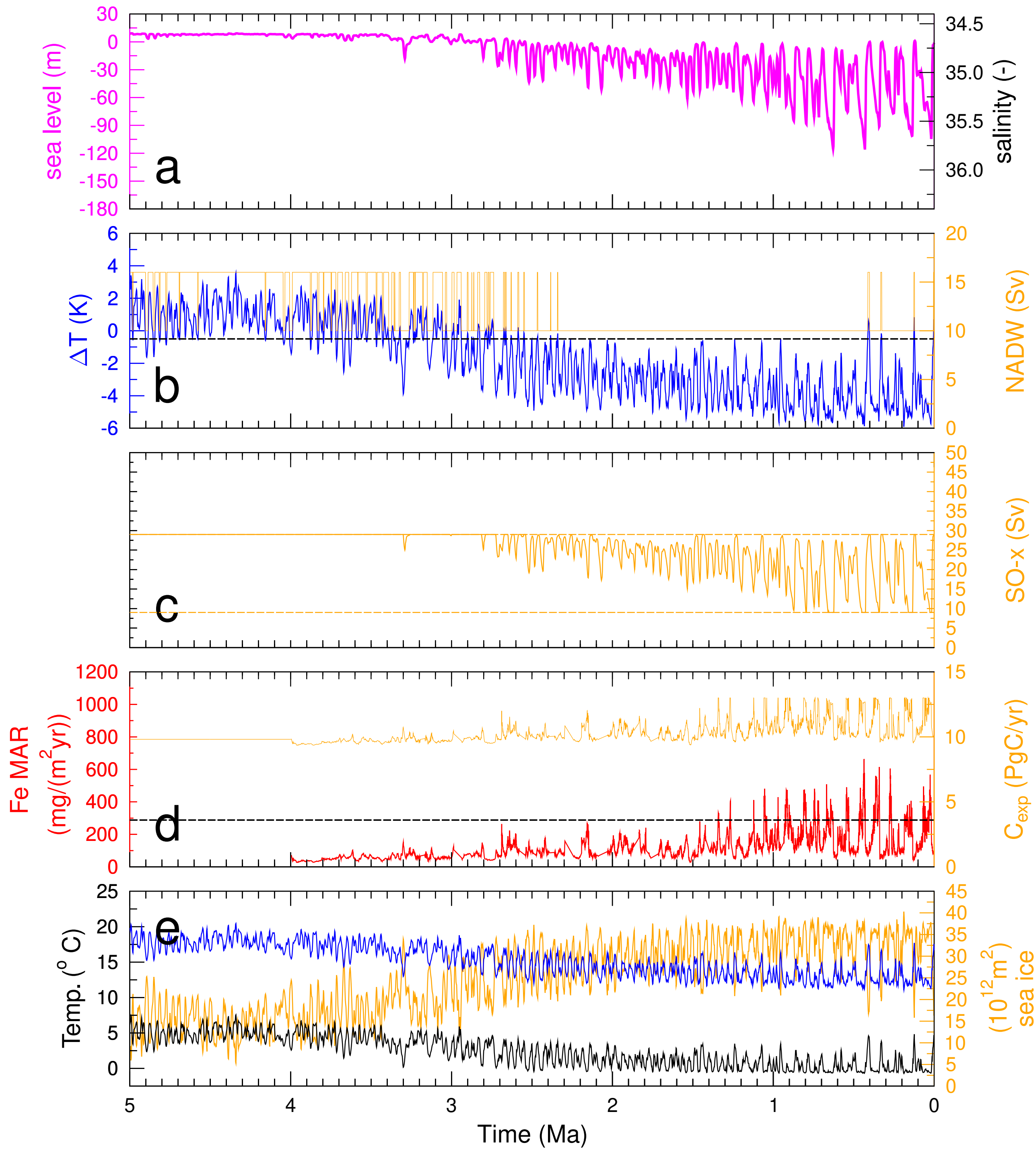

Figure S3. Time-dependent forcing of the model for scenario SEi++V6 (modified from Köhler (2023)). (a) Sea level following de Boer et al. (2014) resulting in the corresponding mean ocean salinity (right y-axis). (b) North Atlantic Deep Water (NADW) formation is either in interglacial or glacial mode, following the globally used temperature record (blue) from Köhler et al. (2015), broken line marks the threshold for switching between both states. (c) Southern Ocean vertical mixing (SO-x: SO surface-to-deep ocean flux, right y-axis) is calculated with upper and lower limitation (9–29 Sv), marked by horizontal lines. Here, the vertical mixing is calculated as function of sea level. (d) Marine biology in the Southern Ocean (SO) is either Fe-limited or Fe-unlimited following Fe MAR in ODP1090 (Martinez-Garcia et al., 2011). The dotted line marks the threshold for switching between both states, leading to global integrated export production of organic matter at 100 m water depth (right y-axis). (e) Ocean temperatures averaged within the model (mean ocean (black), area weighted mean SST (blue)). Right y-axis: global integrated sea ice area.

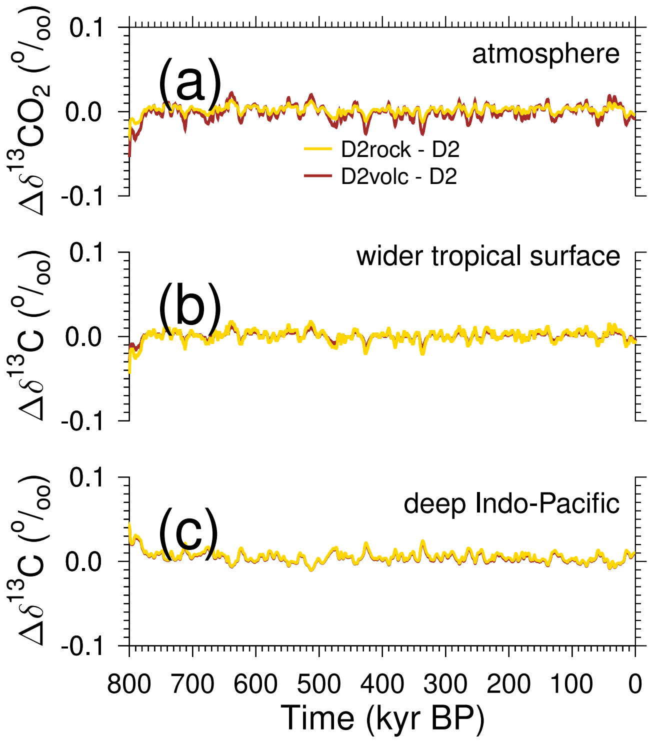

Figure S4. Consistency check. Differences in simulated (a) atmospheric $\delta^{13}CO_2$, (b) wider tropical surface ocean $\delta^{13}C$ and (c) deep Indo-Pacific $\delta^{13}C$ when forcing the model with in post-processing calculated $\delta^{13}C_{rock}$ (D2rock) or the $\delta^{13}C_v$ (D2volc) with respect to D2, the scenarios in which the isotopic signatures have been generated.

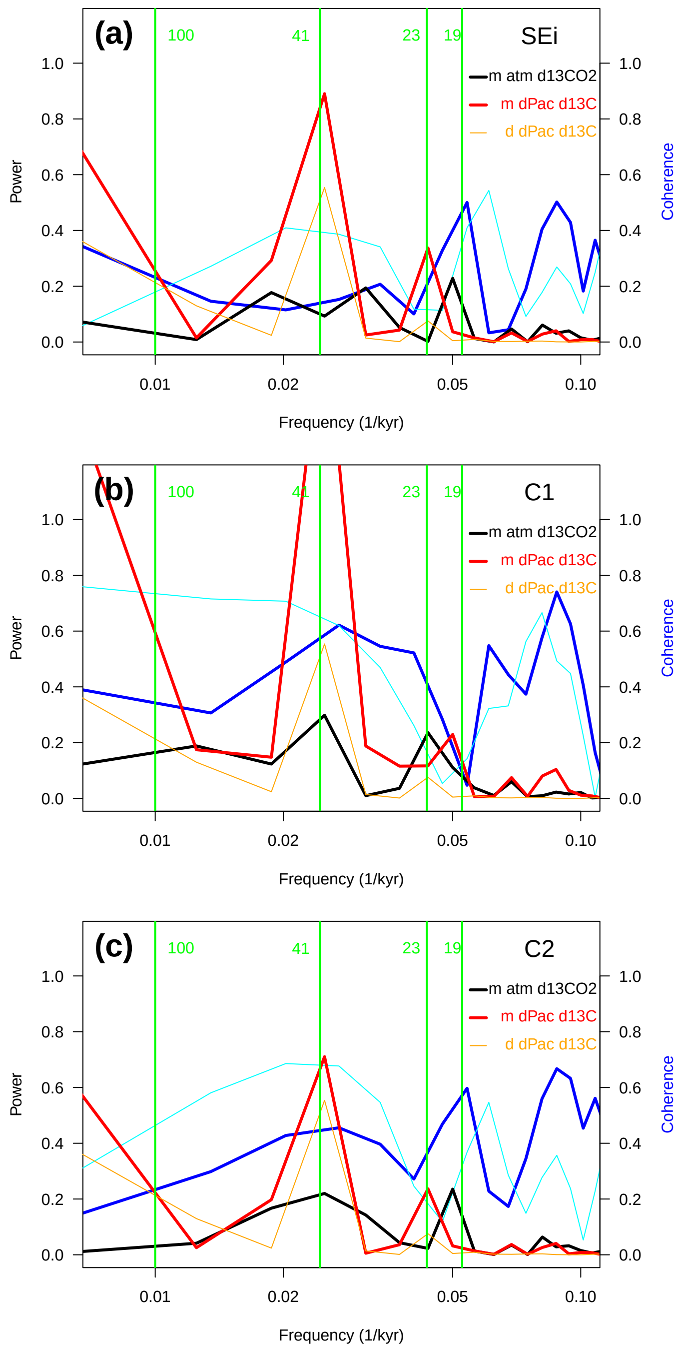

Figure S5. Spectral and coherence analysis for the last 150 kyr of scenarios (a) SEi, (b) C1, (c) C2. Atmospheric $\delta^{13}CO_2$ in the model (m) against deep Indo-Pacific δ^{13}C in the model or in the data (d), where data is the 6 cores stack from Lisiecki (2014).

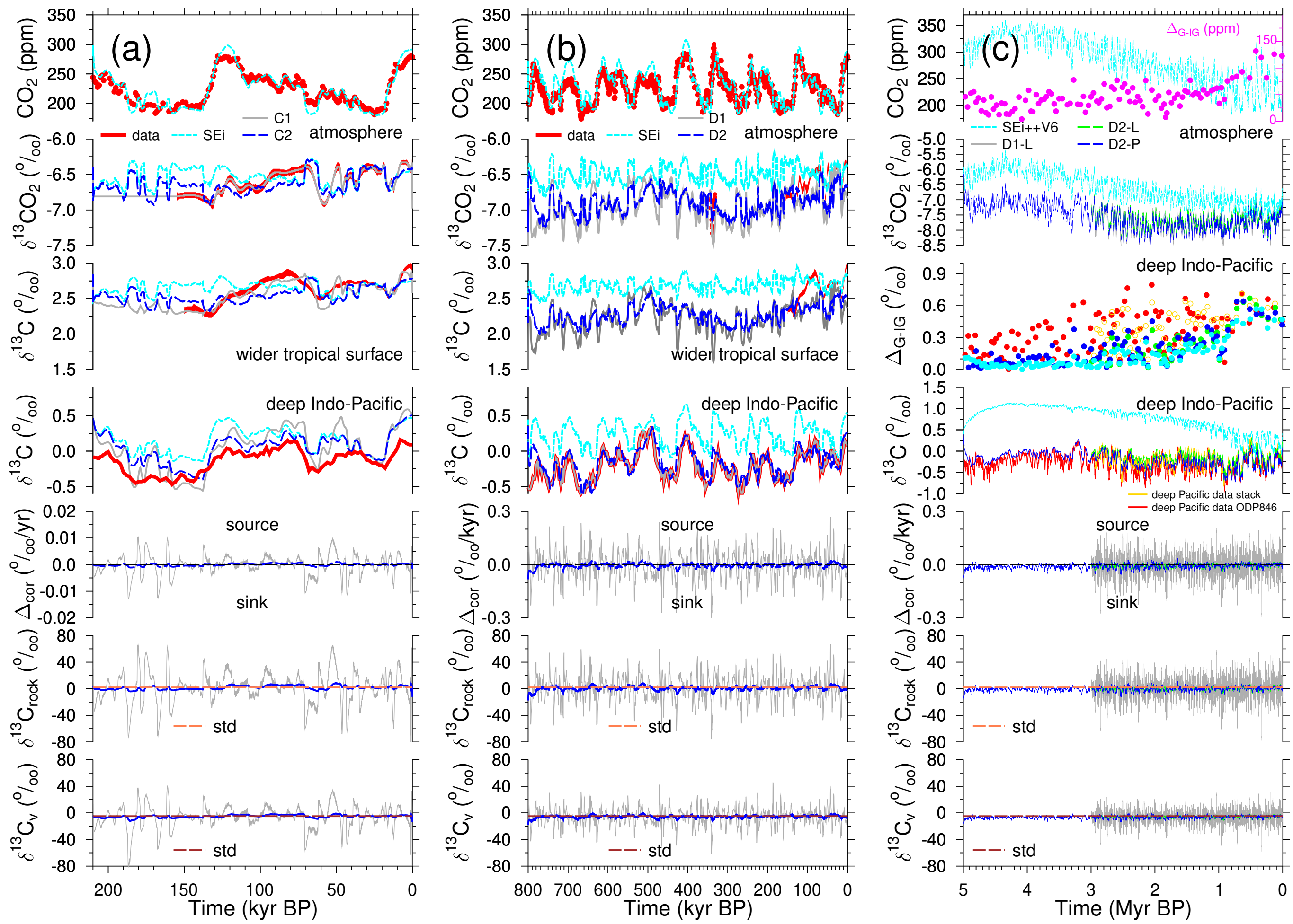

Figure S6. Repetition of Figure 4, but with different y-axes to cover full range of results of Δ_{cor}, $\delta^{13}\mathrm{C}^{\mathrm{hypo}}_{\mathrm{rock}}$ and $\delta^{13}\mathrm{C}^{\mathrm{hypo}}_{\mathrm{v}}$ in the *prescribed* scenarios (C1, D1, D1-L). Closure of the ^{13}C cycle on 405-kyr periodicity. From top-to-bottom: Atmospheric CO_2, $\delta^{13}CO_2$, δ^{13}C in DIC of surface water of the wider tropics, or in the deep Indo-Pacific, Δ_{cor}, $\delta^{13}\mathrm{C}^{\mathrm{hypo}}_{\mathrm{rock}}$, $\delta^{13}\mathrm{C}^{\mathrm{hypo}}_{\mathrm{v}}$ for different scenarios including reconstructions of CO_2 and $\delta^{13}CO_2$ (Bereiter et al., 2015; Eggleston et al., 2016; Krauss et al., 2025), $\delta^{13}\mathrm{C}_{\mathrm{DIC}}$ in the surface ocean of the wider tropics (anomalies to the LGM in the mono-specific stack of *G. ruber*, $\Delta(\delta^{13}\mathrm{C}_{\mathrm{rub}})$ from Köhler and Mulitza (2024)) or in the deep Pacific from the 6 cores stack (Lisiecki, 2014) or ODP846 (Poore et al., 2006). Δ_{cor} is calculated from (a) atmospheric $\delta^{13}CO_2$ or (b, c) from deep Indo-Pacific δ^{13}C. In (c) $\Delta_{\mathrm{G-IG}}$ are included for CO_2 (first row, right y-axis) and (third row) Indo-Pacific δ^{13}C (gold open circles for the 3 Ma-long deep Pacific δ^{13}C stack). No δ^{13}C in DIC of the wider tropical surface ocean is plotted in (c). For $\Delta_{\mathrm{G-IG}}$ the difference between a glacial minima and the subsequent interglacial maxima are calculated following the MIS boundary definition of Lisiecki and Raymo (2005) with points being positioned at mid-transitions.

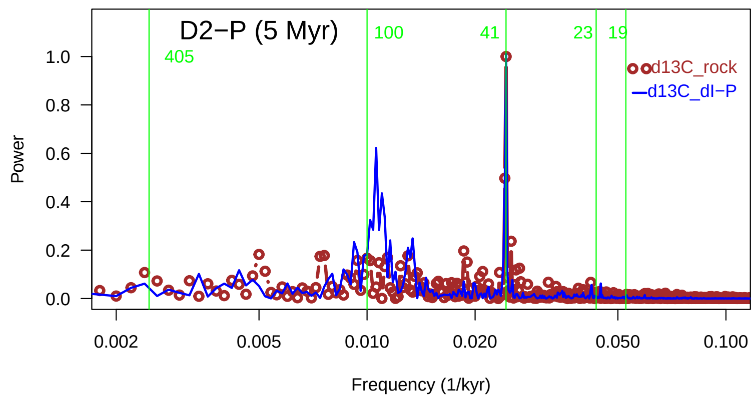

Figure S7. Spectral analysis (normalized power) of $\delta^{13}C_{\mathrm{rock}}$ and of deep Indo-Pacific δ^{13}C of 5-Myr long time series from scenario D2-P.

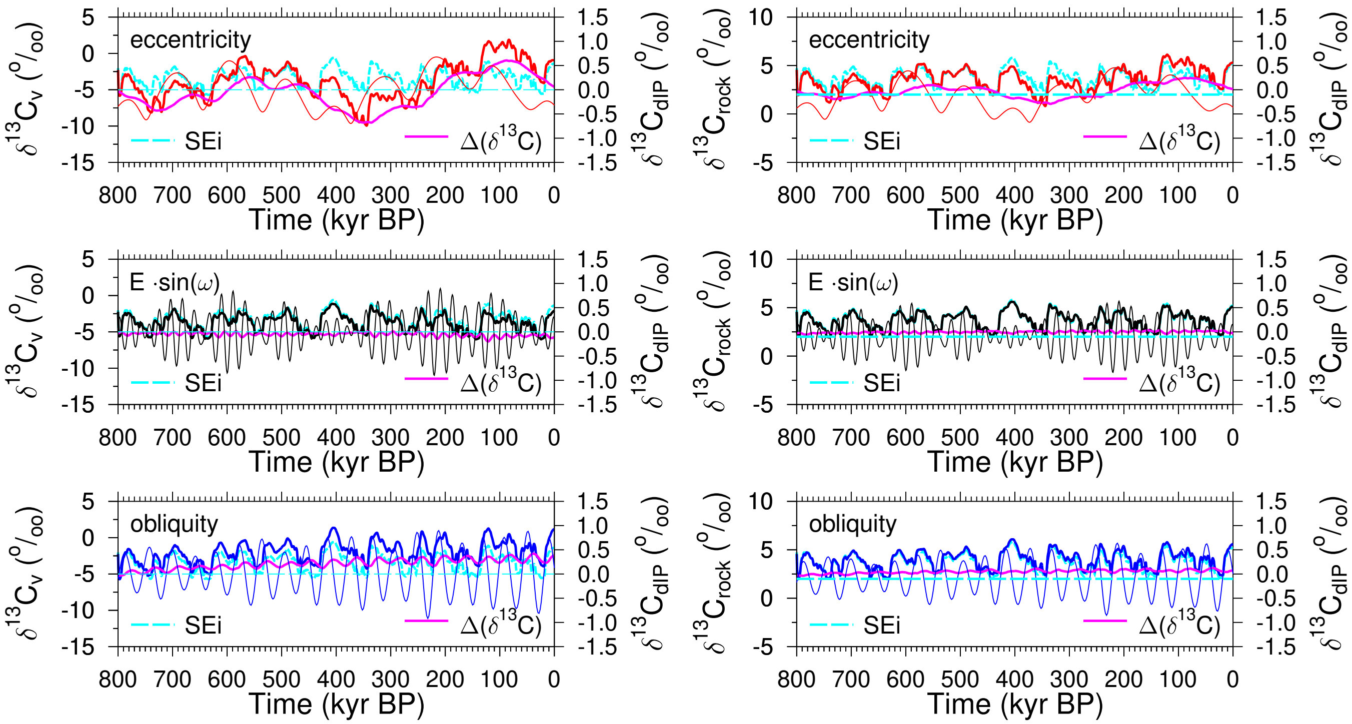

Figure S8. Testing the response of orbitally-forced isotopic signature of geological sources (thin, left y-axes) on deep Indo-Pacific δ^{13}C (thick, right y-axes), applied to otherwise unchanged control run SEi (difference to SEi in magenta). Top: eccentricity; middle: climatic precession ($E \cdot \sin(\omega)$, where E is the eccentricity and ω is the longitude of the perihelion from the moving equinox); bottom: obliquity. Based on orbital time series taken from Laskar et al. (2004).